IN-LINE MONITORING OF DIELECTRIC AND FLUORESCENCE SPECTROSCOPY DURING POLYMER/FILLER COMPOUNDING

Anthony J. Bur, Steven C. Roth, Yu-Hsin Lee, and Natsuko Noda
National Institute of Standards and Technology, Gaithersburg, MD 20899-8542
Michael McBrearty, Chemical ElectroPhysics Corp., Hockessin, DE 19707

Abstract

A new multipurpose instrument has been used to obtain real-time dielectric and fluorescence spectroscopy from polymer resins compounded with inorganic fillers. The instrument, which is mounted at the exit of an extruder, contains a flow-through slit channel that provides a constant geometry platform for dielectric and fluorescence sensors and for other sensors that can be added as needed. The results of real-time monitoring of nylon 6 and ethyl vinyl acetate copolymer (EVA) compounded with organo modified montmorillonite clays will be presented. Real-time dielectric data are corrected for electrode and conductivity effects before analysis yields information about dielectric relaxation phenomena. Significant differences in dielectric dispersion parameters were observed for clay nanocomposites in the aggregate, intercalated and exfoliated states. Fluorescent dyes, doped into EVA copolymer, are being used as molecular probes to study the effects of microstructure conformation on their spectra.

Introduction

In previous publications we described a first generation dielectric sensor that we used for in-line monitoring of extruded polymer resins.[1,2] That sensor is a mono-functional device for measuring dielectric properties only. It consists of a ceramic ring that has interdigitating electrodes deposited on its inside surface. As resin flows through the ring, its dielectric properties are monitored by a fringing electric field that extends into the resin melt. Using this sensor, we reported the results of compounding resins with inorganic fillers.[2]

The interdigitating electrode design has the advantage that the sensor is one-sided and does not involve sensing across the full dimension of the flow stream. However, the interdigitating design has the disadvantage that the sensing electric field is confined to the near surface region. For a 12.7 mm diameter ring with interdigitating electrodes that are separated by 0.33 mm, the field extends only 0.4 mm into the resin melt. Consequently, only 10 % of the cross section of resin flow stream, a thin shell near the surface, is monitored. This is because the strength of the electric field decays from the surface with a characteristic decay length of d/3 where d is the interelectrode separation.[2,3]

Given that 90 % of the flow steam escapes examination with the ring design, we sought to develop a new multifunctional sensor that has a slit configuration. In this paper we will describe the sensor and demonstrate its capabilities as an on-line, real-time sensor of dielectric, rheological and optical properties during the compounding of polymer/clay nanocomposites.

Sensor Design [a]

The slit channel, shown in Figure 1 with approximate dimensions of 2 mm high by 2.8 cm wide by 15 cm long, defines a constant geometry sample cell in which the processed material is characterized by on-line sensing devices. The primary sensor in the channel is the dielectric sensor consisting of interdigitated electrodes that are deposited and fired onto a ceramic substrate that forms one surface of the slit. Other sensors in the current design are pressure and optical sensors situated along the axial dimension of the slit. By keeping the slit height at 2 mm or less, it is possible to fix the interelectrode separation so that the fringing electric field extends significantly into the flow stream interrogating up to 50 % or more of the resin flow. The slit die has a flexible design that permits the addition of new sensors or instrumentation ports, or permits the interchange of sensors to different positions in the slit channel.

Figure 1 is a schematic of the sensor as viewed from the side and front. Two semicircular stainless steel pieces, top and bottom halves, form the cylindrical geometry of the sensor. Its overall dimensions are 12.7 cm diameter by 15.24 cm long (5 inches diameter by 6 inches long), but the cell can be fabricated with a longer length for the purpose of adding additional instrumentation ports. Or, an additional port sector can be added in the sensor train. The sensor housing contains threaded instrumentation ports of the standard half-inch by 20 threads-per-inch type in addition to two cut out chambers for ceramic in-lays that are used for dielectric sensing. The ceramic piece on the bottom is high purity alumina onto which platinum electrodes have been deposited in an interdigitating pattern. The ceramic on top is made from machinable ceramic, has a trapezoidal cross section, and contains a cutout of the slit that is 2 mm deep by 2.8 cm wide extending over the length of the piece, approximately 11 cm. The depth and width dimensions of the slit were machined with an accuracy of 0.012 mm. The trapezoidal cross section serves to hold the

[a] Identification of a commercial product is made only to facilitate experimental reproducibility and to describe adequately the experimental procedure. In no case does it imply endorsement by NIST or imply that it is necessarily the best product for the experiment.

Presented at the Polymer Processing and Engineering Conference, Bradford, UK, July '03

piece into place in the top half stainless steel. A heating jacket surrounds the sensor and temperature is controlled using a thermocouple inserted into the body of the steel housing. A customized interface adapter plate positioned between sensor and extruder establishes the connection to the extruder. This plate contains the appropriate threaded screw holes for the specific extruder being used and contains threaded mounting holes for the bolting the sensor into place.

The alumina ceramic is positioned in a well that has been machined into the bottom half stainless piece and is held mechanically in place by clamping top and bottom halves together. No epoxy or other adhesive is needed. To change ceramic substrates, the alumina block is removed from its well using the lifting bolts on the bottom of the housing to push the block out of the well. It can be replaced with electroded alumina substrates with different electrode patterns that produce fringe electric fields closer and farther from the surface and directed parallel or perpendicular to the flow. Likewise, the ceramic with the slit in the top half of the sensor can be interchanged with pieces having different slit sizes.

A pattern of interdigitating electrodes is shown in Figure 2. Two sets of finger electrodes are interwoven to create the sensor. Each set of fingers is connected to a lead electrode. When an alternating voltage is applied between the electrodes, an electric field fringes between neighboring finger electrodes and extends not only through the alumina ceramic but also into the liquid media flowing above the surface. By measuring the value and phase of the resultant current and subtracting out the current through the alumina, the relative permittivity and dielectric loss of the liquid media can be determined. The electronics detecting circuitry and the software to operate the system is the same as has been used with the dielectric ring sensor and has been described in previous publications.[1,2]

The slit configuration accomplishes two objectives: first, it confines the flowing liquid to a thin ribbon so that a significant fraction of its cross section is intersected by the fringing electric field lines, and second, it is the geometry of a slit die rheometer, i.e. in conjunction with a measurements of the pressure drop across the length of the slit and the flow rate, the viscosity of the material can be determined. For this purpose, a pressure transducer is positioned upstream from the dielectric sensor and yields the value of the pressure drop along the axial length of the slit.

The optics sensor, shown in Figure 3, is situated upstream of the dielectric sensor in the stainless steel housing of the slit die. It consists of a bundle of seven 200 μm core optical fibers that are placed into a sleeved standard half-inch sensor bolt with a sapphire window at its end. It operates in one of two possible modes: to measure light transmission through the resin in the slit, or to measure the fluorescence from a fluorescent dye that has been doped into the resin matrix.

In the transmission mode, one of the fibers transmits light from the light source through a focusing lens, the sapphire window, the flowing resin, reflects off the far stainless steel surface, and reverses its path through the material, sapphire window and lens. The reflected light is collected by the other six fibers and is transmitted to the photomultiplier detector. For fluorescence measurements the collection optical fibers are connected to a spectrometer as shown in Figure 4.

Optional sensor port sectors, shown in Figure 5, can be added in-line, sandwiched between the slit die and the interface plate. Ancillary sensors such as UV or infrared absorption, optical microscope, ultrasonic velocity etc. can access the resin flow stream at this site. The optional sectors can be added or removed from service in accordance with the needs of the experiment and they can be customized to enhance sensor performance, e.g. installing optical windows for microscopy experiments.

Fluorescence Measurements

Fluorescent dyes are employed in order to probe the molecular environment of the composite, e.g. temperature, molecular orientation, and microstructure conformation. The dye is chosen according to the experimental objective and doped into the resin at concentrations less than 10^{-5} mass fraction of dye in the resin. Excitation light is transmitted to the sensor via a single 200 μm fiber and fluorescence is collected by six 200 μm core fibers and delivered to a spectrometer or to filtered photomultiplier tubes. For temperature measurements, a dye whose spectrum is sensitive to changes in temperature is chosen. The technique is based on the ratio of fluorescence intensities at different wavelengths and employs the optical equipment shown in Figure 5. The temperature measuring method has been described in detail in references 4 and 5. The fluorescence spectra can also reveal information about microstructure via wavelength or intensity shifts in the spectra caused by the state of the microstructure.

Dielectric Measurements

When a polymer melt is subjected to an electrical field, bound charges are displaced and dipoles are oriented. Measurements made as a function of frequency of applied electric field and temperature yield basic information about molecular dynamics, ionic conductivity, thermally activated processes, and the role of microstructure on the development of interfacial polarization. The behavior is described by the complex relative permittivity ε* where

$$\varepsilon^* = \varepsilon' - i\varepsilon'' \qquad (1)$$

The real part of the relative permittivity ε′ is associated with the polarization or capacitance of the material and the imaginary part ε″, the dielectric loss, is associated with its conductance.

When measuring the dielectric properties of a polymer melt at elevated processing temperatures, ion conductivity becomes a prominent feature of the behavior. This is particularly true when fillers containing ionic species are compounded with a resin matrix. In some cases the ion conductivity is so large that it overrides molecular dipolar and microstructural relaxation processes. In general the conductivity σ can include a frequency independent component σ_{DC} associated with the drift of unbound charges and also a frequency dependent component σ_r related to dielectric relaxation,

$$\sigma = \sigma_{DC} + \sigma_r \quad (2)$$

and

$$\varepsilon'' = \frac{\sigma_{DC}}{\omega \varepsilon_o} + \varepsilon_r'' \quad (3)$$

where $\omega = 2\pi$ x frequency, $\varepsilon_0 = 8.854 \times 10^{-12}$ F/m and ε_r'' is the frequency dependent part of the dielectric loss. Ionic conduction also contributes to the real part of the relative permittivity as electrode polarization or as interfacial polarization. Both of these phenomena usually occur at low frequency when ions can follow in phase with the applied electric field and accumulate at the electrode or, in a heterogeneous mixture, at the interface between components of different dielectric constant. The frequency dependence of interfacial polarization is known as Maxwell-Wagner relaxation. For composite materials, a distribution of permittivities and conductivities produces a distribution of relaxation times, effects that are the focus of our effort to monitor the dielectric properties of polymer composites.

Materials

To demonstrate the operation of the slit die sensor, we present real-time monitoring data for compounding two resins, nylon 6, Capron 8200 from Honeywell, and ethyl vinyl acetate copolymer (EVA), ELVAX 460 from DuPont with 18% vinyl acetate. These resins were compounded with two montmorillonite clays, Cloisite 30B, and Cloisite 15A from Southern Clay Products. The clays are modified clays whereby natural clays are ion exchanged with quartra ammonium ions containing organic appendages that make the clay more hydrophobic and compatible with organic polymers. In the ion exchange process the quartra ammonium ions occupy the gallery between silicate layers priming the clay for exfoliation or intercalation when compounded with the resin matrix.[6] The powdered clay was compounded with the polymer at 4 % and 2 % mass fraction of clay in the polymer. Compounding was carried out using an 18 mm Haake Reocord model 9000 twin screw extruder operating at 60π rad/min (30 rpm). The fluorescent dye, benzoxazolyl stilbene (BOS), was obtained from Aldrich Chemical Co.

Standard uncertainties for the measurements were 1 °C for temperature and 35 kPa (5 psi) for pressure. The standard uncertainty in relative permittivity is 0.01 and for conductivity it is 1×10^{-11} S/m. The relative standard uncertainty in fluorescence intensity is 0.5 %.

Results and Discussion

Dielectric Monitoring. Figure 6 shows real-time dielectric data for extrusion of nylon 6 (neat) and for nylon 6 compounded with 4 % Cloisite Clays 30B and 15A. Compounding was carried out at 240 °C. Relative permittivity and dielectric loss are plotted versus time for fifteen different frequencies ranging from 50 Hz to 100 kHz. The experiment started with extrusion of the neat resin followed by compounding and extrusion of resin with 4 % mass fraction of 30B clay in the resin and ending with 4 % mass fraction of 15A clay in the resin. At t = 0 s, the neat polymer entered the electrode region of the dielectric sensor and was extruded for approximately 1430 s, at which time resin pellets mixed with 4 % mass fraction of 30B clay were added to the feeder. Permittivity and conductivity began to increase as the mixture filled the slit region. After significant transition time, the data reached a plateau value. The transition is associated with time it takes the clay/polymer mixture to completely fill the sensing region, particularly at the surface near the electrodes. Between 4150 s and 4400 s resin with 4 % mass fraction of 15A clay was introduced and its dielectric properties reached a new plateau at t = 4800 s. The scatter in the data at 50 Hz is due to variations in pressure and concentration of the clay. The dielectric constant at 50 Hz is particularly sensitive to the ion or clay concentration which varies somewhat as the resin pellets/clay powder mixture is fed into the extruder.

The difference in relative permittivity at low frequency (50 Hz) and high frequency (10^5 Hz) is called the dielectric dispersion. We see that the dispersion for the clay/polymer nanocomposite is considerably larger than that for the neat polymer. This is because clay particles in the resin introduce ionic species that contribute to conductivity and polarization over and above that which is present in the neat resin.

When plotted versus frequency (Figure 7), the measured dielectric data, ε'_{meas} and ε''_{meas}, are monotonically decreasing with frequency and show no discernible features. In spite of the bland appearance of these curves, they contain a wealth of dynamic information. This is because dielectric data as a function of frequency must follow well established functional behavior. The experimental data are analyzed using a global fitting procedure that takes into account DC conductivity, electrode polarization, and dielectric relaxation behavior. The phenomenon of electrode polarization is prominent in polymer melts especially impacting the low frequency data where it dominates the measurement. Figure 8 depicts a sample sandwiched between electrodes that express electrode polarization due the pileup of ions at the electrode surfaces. The situation can be described as an electrode admittance Y_{el} in series with the sample admittance Y_s. These admittances add to yield the apparent admittance Y_{app} where

$$Y_{app} = G_{app} + j\omega C_{app} = \frac{Y_{el} Y_s}{Y_{el} + Y_s} \quad (4)$$

and

$$\varepsilon'_{app} = \frac{C_{app}}{C_o} \text{ and } \varepsilon''_{app} = \frac{G_{app}}{\omega C_o} \quad (5)$$

Here, G_{app} is the apparent conductance, C_{app} is the apparent capacitance, C_o is the empty cell capacitance, and ε'_{app} and ε''_{app} are the apparent real and imaginary parts of the dielectric constant. Carrying out the algebraic manipulations of the right hand side of equation (4) yields

$$\varepsilon'_{app} = \frac{C_{app}}{C_o} = \frac{\varepsilon'_c \frac{G_{elr}^2}{\omega^2} + \varepsilon''^2_c C_{elr} + \varepsilon'_c C_{elr}^2 + \varepsilon'^2_c C_{elr}}{\left(\frac{G_{elr}}{\omega} + \varepsilon''_c\right)^2 + \left(C_{elr} + \varepsilon'_c\right)^2} \quad (6)$$

and

$$\varepsilon''_{app} = \frac{G_{app}}{\omega C_o} = \frac{\frac{G_{elr}^2}{\omega^2}\varepsilon''_c + \varepsilon''^2_c \frac{G_{elr}}{\omega} + \varepsilon'^2_c \frac{G_{elr}}{\omega} + \varepsilon''_c C_{elr}^2}{\left(\frac{G_{elr}}{\omega} + \varepsilon''_c\right)^2 + \left(C_{elr} + \varepsilon'_c\right)^2} \quad (7)$$

where ε_c' and ε_c'' are the calculated real and imaginary parts of the sample dielectric constant, and G_{elr} and C_{elr} are the reduced conductance and capacitance of the electrode impedance, $G_{elr} = G_{el}/C_o$ and $C_{elr} = C_{el}/C_o$.

In our analysis of the data, ε'_{app} and ε''_{app} are compared to the measurement by fitting equations (6) and (7) to ε'_{meas} and ε''_{meas} using a non-linear fitting routine. We note that ε'_{app} and ε''_{app} are functions of both ε_c' and ε_c'' so that the fit to the measured quantities involves a simultaneous minimization of both ε_c' and ε_c''. Aside from G_{elr} and C_{elr}, the fitting parameters include those of the Cole-Cole equation for dielectric dispersions,

$$\varepsilon^* = \varepsilon_\infty + \sum_j \frac{(\varepsilon_o - \varepsilon_\infty)_j}{\left[1 + (i\omega\tau_j)^{1-\alpha_j}\right]} \quad (8)$$

where $(\varepsilon_o - \varepsilon_\infty)_j$ is the strength of the jth dispersion, α_j is the jth relaxation time distribution parameter and ε_∞ is the high frequency dielectric constant.

Our criterion for the fit of ε'_{app} and ε''_{app} to ε'_{meas} and ε''_{meas} was 1% difference or less between measured and calculated quantities. The fits, shown as the solid line curve in Figure 9, yielded two dispersions for the filled nylon but only one dispersion for the neat resin. The high frequency dispersion in the neat and in the 30B and 15A nanocomposites is macromolecular motion associated with the onset of the glass transition in nylon 6 (T_g = 50 °C). A second dispersion seen only in the nanocomposite materials is identified as a Maxwell-Wagner (MW) interfacial dispersion associated with polymer/clay interfaces. As noted in Table 1, the interfacial dispersion has very large relaxation strengths $\Delta\varepsilon$ that can only be achieved with buildup of ionic charge at clay/polymer interfaces. The characteristics of the MW dispersion can be used to identify microstructure, nylon 6/30B having exfoliated microstructure and nylon 6/15A having aggregate microstructure. Their MW relaxation frequencies differ by nearly an order of magnitude with the 30B nanocomposite having the lowest value of f_2.

The MW relaxation frequencies can be interpreted in terms of an RC time constant that describes the conduction of ions through a resistive resin matrix to the surface of the silicate clay particle. The silicate clay particle behaves as a capacitor. Thin exfoliated silicate flakes have high capacity that results in a large RC time constant and low MW relaxation frequency as we observed for the NY6/30B exfoliated nanocomposite.

	NY 6 neat	NY 6/15A	NY6/30B
Log f_1	2.40	2.79	2.64
Log f_2 MW		1.98	1.10
$\Delta\varepsilon_1$	440	1400	1600
$\Delta\varepsilon_2$ MW		17,000	18,000
α_1	0.168	0.10	0.02
α_2 MW		0.16	0.32
σ S/m	3.33E-04	1.44E-03	1.20E-03

Table 1. Results from global fitting of dielectric data

Fluorescence Monitoring. Both dielectric data and fluorescence spectra were measured for EVA compounding, but only the fluorescence data will be reported here. Benzoxazolyl stilbene (BOS) was doped into the EVA copolymer at 10^{-5} mass fraction of dye in the resin by extruding the resin pellets and dye powder together. The constant steady state fluorescence intensity that we observed indicated a uniform distribution of dye. Wide angle x-ray and transmission electron microscope (TEM) observations verify that EVA with 15A clay adopts intercalated microstructure upon compounding at 194 °C. From x-ray data, the intercalation of EVA into the clay galleries expands the galleries between silicate layers by 20 %. The x-ray and TEM observations of EVA/30B clay microstructure show that 30B clay remains in the aggregate state upon mixing with EVA.

In Figure 10, we display three spectra for BOS in neat EVA, in EVA with 4 % mass fraction of 15A clay, and in EVA with 4 % mass fraction of 30B clay. The spectra for BOS in the neat resin and in the EVA/30B nanocomposite is identical with our observation of spectra for BOS dissolved in polar solvents such as chloroform. We conclude that free BOS dye in EVA/30B composite is not impacted by the presence of clay particles in the aggregate state.

However, the intercalated condition of the EVA/15A nanocomposite causes a radical change in the BOS spectra. Such shifts in the spectrum can occur as a result of the change in the internal electric field that the dye experiences in its local environment. For a dye molecule that is intercalated in the clay galleries, the difference between the organic matrix resin environment and inorganic polar clay gallery can mean a difference as large as a factor of 1.5 in the internal electric field, thus changing the magnitude of the dye's Stokes shift. Because the clay concentration in the matrix is several orders of magnitude greater than the dye, there exists a large clay surface area for absorption of the relatively few dye molecules. Our working hypothesis is that the dye is associated in the intercalated regions of the clay and this produces the spectral shift that we observe.

Conclusions

The operation of a new dielectric slit die sensor has been demonstrated. It is a multi-functional device that delivers a package of data about the processed resin. Global analysis of dielectric spectra yields characteristic relaxation parameters that are associated with specific microstructure. The addition of fluorescent probe molecules to composites permits the examination of microstructure via changes in the fluorescence spectra. Future work will focus on the relationships between fluorescence, dielectrics and nano-composite microstructure.

References

1. S. Perusich and M. McBrearty, Polym. Eng. Sci. **40**, 214 (2000).
2. A. J. Bur, S. C. Roth and M. McBrearty, Rev. Sci. Instr. 73, 2097 (2002).
3. M. C. Zaretsky, P. Li, and J. R. Melcher, IEEE Trans. Elect. Insul. **24**, 1159 (1989).
4. A. J. Bur, M. G. Vangel and S. C. Roth, Appl. Spect. **56**, 174 (2002).
5. A. J. Bur, M. G. Vangel and S. C. Roth, Polym. Eng. Sci. **41**, 1380 (2001).
6. H. R. Dennis, D. L. Hunter, D. Chang, S. Kim. J. L. White, J. W. Cho, D.R.Paul, Polymer 42, 9513 (2001).

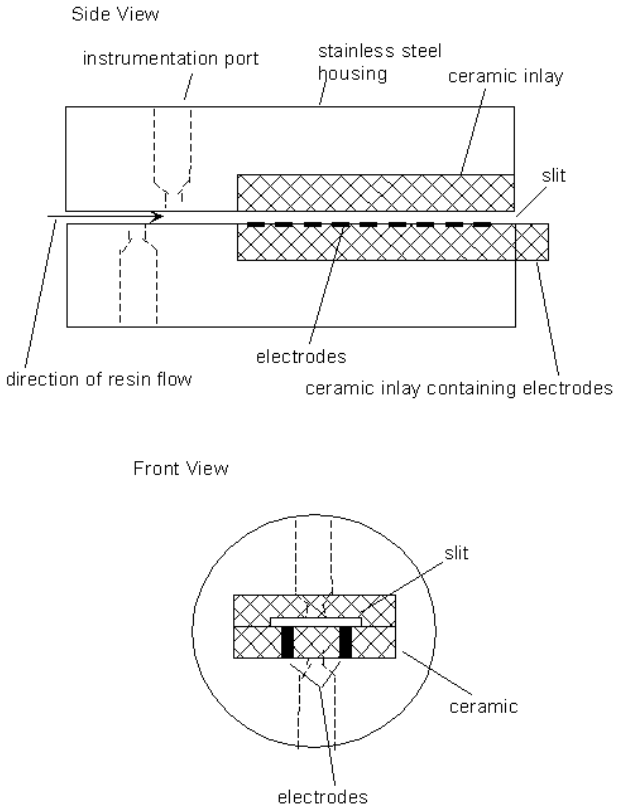

Figure 1. Side and front views of the dielectric slit die.

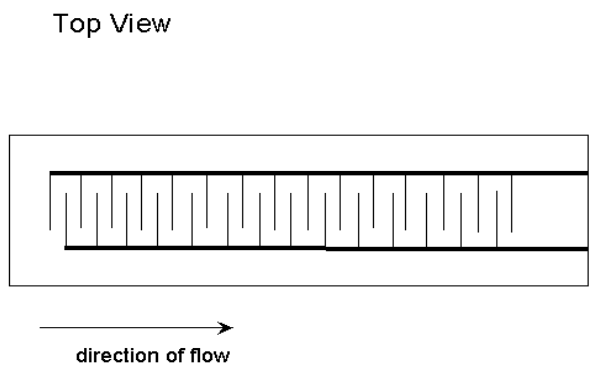

Figure 2. The pattern of interdigitating electrodes.

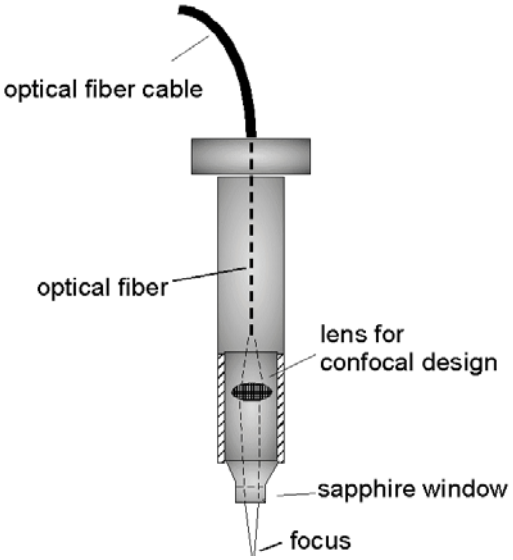

Figure 3. The standard half-inch bolt modified to receive optics.

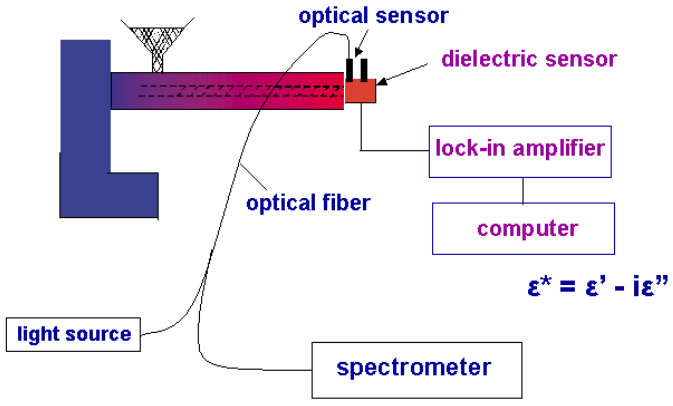

Figure 4. Optics light source and detection setup

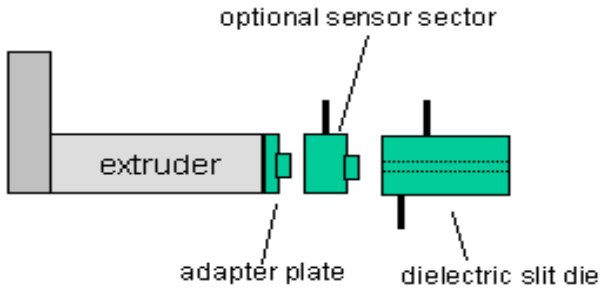

Figure 5. The position of the optional sensor port is shown

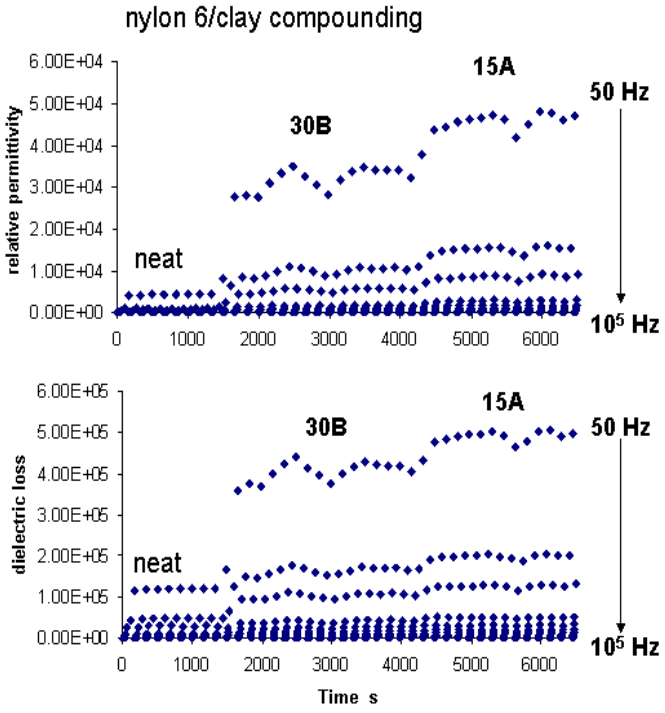

Figure 6. Real part, relative permittivity and imaginary part, dielectric loss, are plotted versus time for compounding of nylon 6 with 30B and 15A clays.

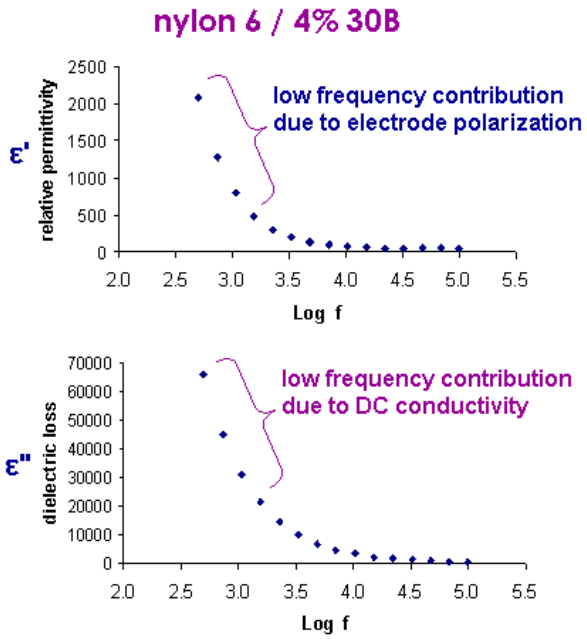

Figure 7. ε′ and ε″ versus log frequency for nylon 6 with 4 % 30B clay and processed at 240 °C

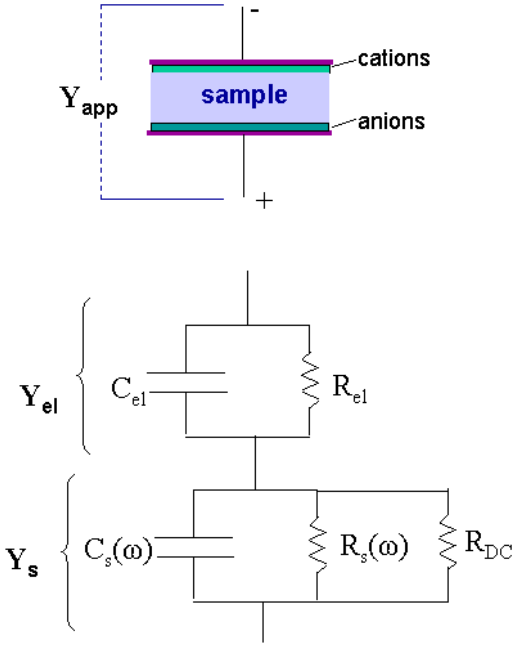

Figure 8. A schematic of electrode polarization and its equivalent circuit are shown.

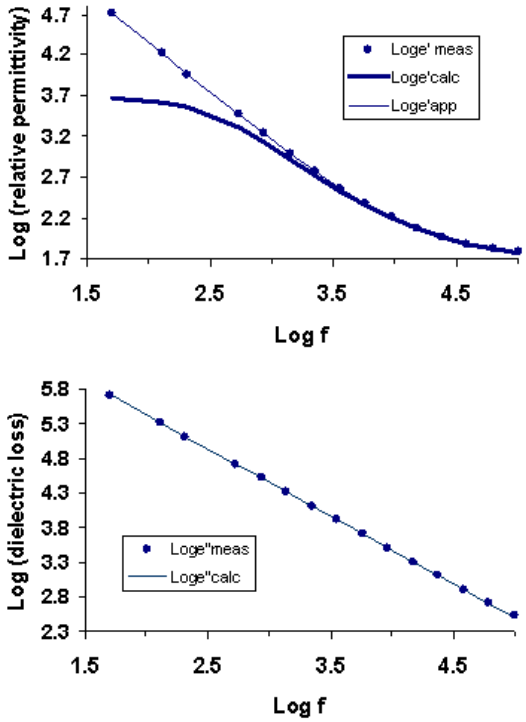

Figure 9. Relative permittivity and dielectric loss are plotted versus log frequency for nylon 6 compounded with 15A clay. Points are measured data. Thin lines are fits to the data. Thick line is the calculated ε′ after correcting for electrode polarization.

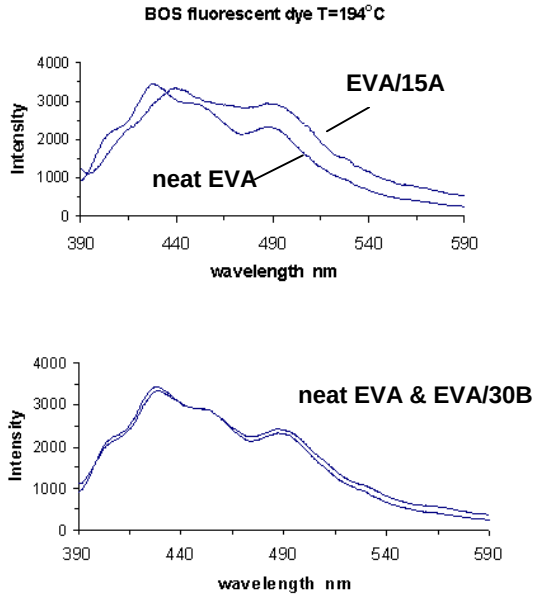

Figure 10. Fluorescence spectra for EVA copolymer doped with BOS dye and compounded with 15A and 30B clay